Solid State Nuclear Magnetic Resonance 110 (2020) 101700

Contents lists available at ScienceDirect

Solid State Nuclear Magnetic Resonance

journal homepage: www.elsevier.com/locate/ssnmr

Structural and functional synthesis of the continuous wave NQR temperature sensor with increased conversion linearity

A. Samila [a,*], I. Safronov [a], O. Hotra [b]

[a] Department of Radio Engineering and Information Security, Yuriy Fedkovych Chernivtsi National University, Kotsjubynskyi 2, 58012, Chernivtsi, Ukraine
[b] Institute of Electronics and Information Technology, Lublin University of Technology, Nadbytrzycka 38A, 20618, Lublin, Poland

ARTICLE INFO

Keywords:
nuclear Quadrupole resonance
Marginal oscillator
Amplitude demodulation
Temperature sensor

ABSTRACT

The paper describes development of the detailed structure and circuit diagrams of the continuous wave NQR temperature sensor with increased conversion linearity. It is experimentally established that at amplitude modulation of 40% and change of input voltage in the range of 20–1000 mV, the circuit of a symmetric marginal oscillator with a linear active demodulator provides better linearity of transfer characteristic than the circuits of asymmetric marginal oscillators with JFET or diode detectors. As a thermometric substance of the proposed NQR sensor, copper oxide Cu_2O was used, which is characterized by a strong temperature dependence of the resonance frequency of ^{63}Cu NQR. In contrast to ^{35}Cl NQR in $KClO_3$, for cuprous oxide the temperature dependence of ^{63}Cu NQR frequency in the frequency range 26.621–25.658 MHz is linear in the temperature range 100–390 K. It is experimentally confirmed that the use of a low mass sample (less than 200 mg) as a thermometric substance of the proposed NQR sensor is quite sufficient for successfully observation of the resonance line at the SNR equal to 9.1 dB.

1. Introduction

There are continuous wave (CW) and pulsed methods for observing nuclear quadrupole resonance (NQR) signals in the frequency range from ~2 to 1000 MHz. Despite the intensive development of pulsed methods in resonance radiospectroscopy, CW methods have not lost their relevance and are still used in laboratory practice. This is especially true of NQR spectroscopy, where the absence of a strong external magnetic field makes them attractive and accessible to researchers. The results obtained with the help of NQR are unique and valuable in the study of the structure of materials. Great contribution to the development of theoretical foundations and scientific and technical basis of NQR thermometry was made by such scientists as R.T. Pound, F.N.H. Robinson, Michael S. Adler, Tara P. Das, V.S. Grechishkin, T.N. Rudakov and others [1–4].

Marginal oscillators based on junction gate field-effect transistor (JFET) have been widely used by scientists in recent decades to observe the methods of continuous wave spectroscopy of NQR, nuclear magnetic resonance (NMR) and electron paramagnetic resonance (EPR) signals [5–21]. Compared to other similar devices, such circuits are characterized by simplicity, reliability and high sensitivity [7–11]. Despite the fact that the principle of modern radio spectrometers is based on the methods of pulse Fourier transform spectroscopy, marginal oscillators can be effectively used in the development of high-sensitivity and high-precision NQR sensors of physical quantities (temperature, pressure, magnetic field, etc.) that do not require calibration and periodic verification. Unlike pulse Fourier transform NQR spectroscopy, where the sample is exposed to strong radio frequency radiation, continuous wave spectroscopy uses weak radio frequency radiation, which has little effect on the parameters of the sample crystal lattice, and therefore makes it possible to significantly increase the accuracy of the NQR sensor [12–17]. The potential use of such sensors is possible in distributed sensor networks and devices of the Internet of Things physical link. Spintronics is also an important application area of marginal oscillators [22].

From the analysis of scientific works it follows that the most well-known methods of synthesis of circuit diagrams of marginal oscillators are based either on cumbersome analytical calculations using the classical theory of signal generation and nonlinear systems, or on the results of numerous experimental studies [18–20]. In this case, in the majority of cases, the increase in sensitivity is achieved mainly by reducing the intrinsic noise of the circuit and weakening the external interference [21]. The aim of this work is develop circuit diagrams of marginal oscillator NQR sensor with increased conversion linearity using simulation results. Cuprous oxide (Cu_2O) was chosen as a research object of the

* Corresponding author.
E-mail address: a.samila@chnu.edu.ua (A. Samila).

https://doi.org/10.1016/j.ssnmr.2020.101700
Received 24 July 2020; Received in revised form 10 October 2020; Accepted 2 November 2020
Available online 12 November 2020

developed temperature sensor. To a large extent, this choice is due to the ability to provide a high frequency of cuprous oxide, which in turn provides high reproducibility of the response signal line width, as well as a relatively narrow absorption line width (~10 kHz) and high temperature sensitivity ~ 4–5 kHz/°C.

2. Analysis of amplitude demodulation methods in marginal oscillators

Among the known circuit diagrams of marginal oscillators, there are several basic ones, the difference between which is mainly in the method of introducing the feedback required for the occurrence of self-oscillations [7–11,18–21]. These devices for amplitude demodulation of absorption signal employ conversions in a nonlinear element of the marginal oscillator – a transistor or a semiconductor diode. In each case, with a successful design, careful selection of electronic components and modes of operation of the oscillator with self-excitation, a fairly high sensitivity of detection of absorption signals can be achieved.

Ref. [7–9,18–21] describe the use of a nonlinear converter on JFET for amplitude demodulation. In addition to the above strong points, this demodulator has disadvantages. It is, first of all, high coefficient of nonlinear distortion of the output signal, as well as the need to constantly adjust the position of the operating point of the transistor when changing the mode of operation of the marginal oscillator. The use of an amplitude demodulator on a semiconductor diode to detect the NQR signal is described in Ref. [7]. Due to the use of a high-frequency cascade amplifier, this diode demodulator operates in strong signal mode. A similar solution is also described in Ref. [10]. The introduction of an additional amplification stage improves the linearity of the transfer characteristic of the demodulator.

Simulation Program with integrated circuit emphasis (SPICE) simulation was performed to synthesize the amplitude demodulator circuit and study its transfer and noise characteristics (Fig. 1).

SPICE simulation was performed in the Cadence OrCAD software. The noise characteristics of the JFET based and diode based amplitude demodulators are shown in Fig. 2 and Fig. 3. In the range of input voltages 0.1–2.2 V, the active diode demodulator provides better linearity of the transfer characteristic than the JFET based demodulator. The SPICE simulation results showed that for the circuit shown in Fig. 1B the harmonic factor is 33% smaller (at $m = 10\%$) compared to the harmonic factor for the model shown in Fig. 1A.

Active amplitude demodulators are known to have a number of advantages over passive ones, in particular, have better linearity of the transfer characteristic. In order to study the characteristics of the active amplitude demodulator, its SPICE model was developed (Fig. 4).

The circuit contains a half-wave rectifier on the operational amplifier (op amp) U1 and an adder on the op amp U2. With a positive polarity of the input voltage, U1 works as an inverting amplifier.

The simulation results of the linear active amplitude demodulator are shown in Fig. 5. The results of SPICE simulation showed that the linear active amplitude demodulator circuit is not inferior in noise characteristics to the JFET or diode demodulators, however, it provides better linearity of the transfer characteristic in the input voltage range of 20–1000 mV. The minimum value of the detected signal (at a carrier of 20 MHz and a modulation frequency of ~1 kHz), which was observed without significant distortion was 1.8%.

3. The principle of implementation of the NQR sensor

The purpose of the experiment was to determine the minimum mass of a thermometric substance which can be precisely detected using the proposed NQR sensor (Fig. 6).

3.1. Symmetrical marginal oscillator

In the process of analysis conducted on the basis of equivalent low-signal circuits and mathematical modeling, the dependences of the noise factor and sensitivity on the amplitude of radio frequency (RF) oscillations for asymmetric and symmetric circuits of marginal oscillator were obtained [21]. A common disadvantage of both circuits is the deterioration of noise characteristics at low levels of generation voltage (below 100 mV). However, with a decrease in the amplitude of RF oscillations, there is an intensive increase in the sensitivity of the marginal oscillator. It is the relationship between these two factors that must be taken into account when setting the operating modes of the circuit.

It was investigated that for BF245C transistors at a carrier frequency of 26 MHz, resonance modulation frequency of 140 Hz, and voltage of generated oscillations on the 800 mV circuit, the noise factor for the symmetrical circuit decreased by 8.5%, and the sensitivity increased by 4.7%. It is obvious that the increase in the sensitivity of symmetric circuits allows observing lower concentrations of the studied nuclei.

Fig. 7 shows the circuit diagram of a symmetrical marginal oscillator [21]. As a threshold oscillator, a two-cycle RF source voltage repeater was used [19]. The specific feature of the proposed circuit is its symmetrical structure with respect to low-frequency (LF) signal. For the RF signal, this is a high-frequency amplifier with positive feedback, and for the LF component, this transistor circuit (Q1, Q2) is, in fact, a differential amplifier. This makes it possible to maintain the symmetry of the circuit while further amplifying the absorption signal. The symmetrical structure of the circuit also significantly reduces the influence of external noise – electromagnetic, acoustic and vibration disturbances to which such circuits are very sensitive, especially if they operate near the threshold of generation failure.

The output of the repeater is loaded on the capacitor C8, whereby the sources of transistors Q1, Q2 are distributed according to RF by coils L3, L5. Oscillations at the resonant frequency are excited by positive

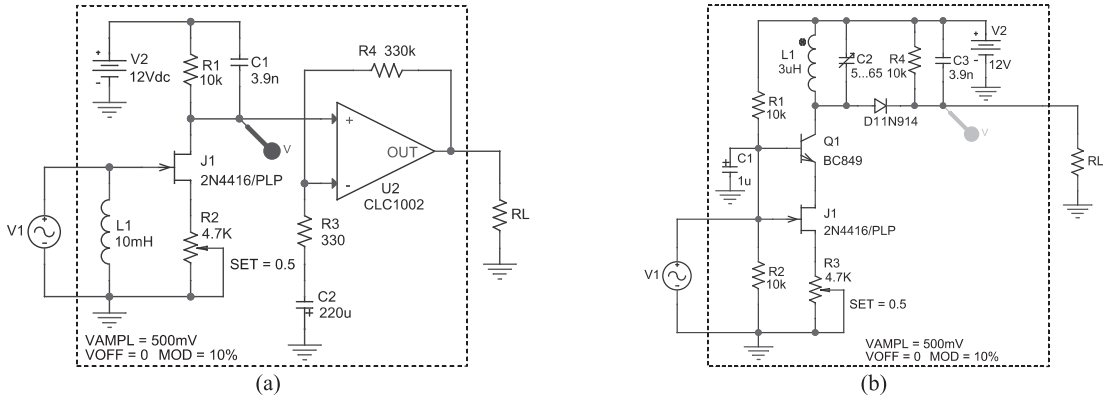

Fig. 1. SPICE models of the amplitude demodulators: A – built on JFET, B – built on diode.

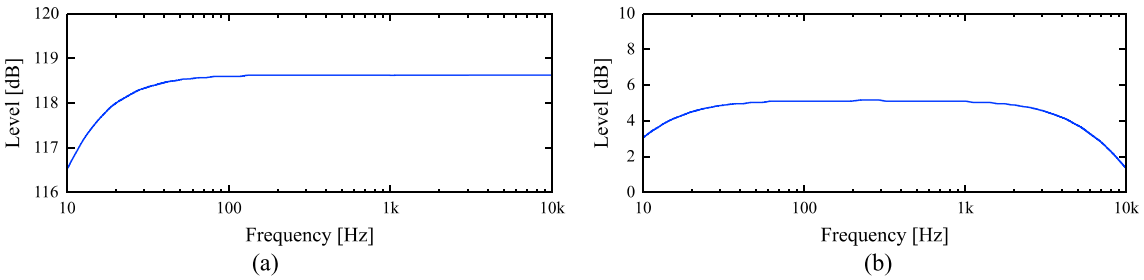

Fig. 2. Simulation results of the JFET based amplitude demodulator: A – signal-to-noise ratio (SNR), B – noise figure.

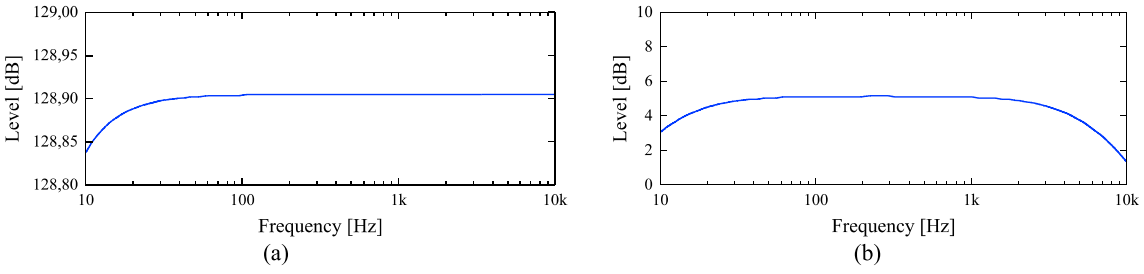

Fig. 3. Simulation results of the diode based amplitude demodulator: A – SNR, B – noise figure.

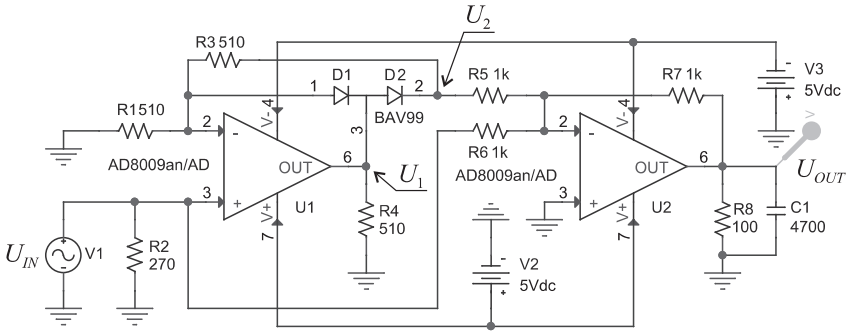

Fig. 4. SPICE model of the op-amp based linear active amplitude demodulator.

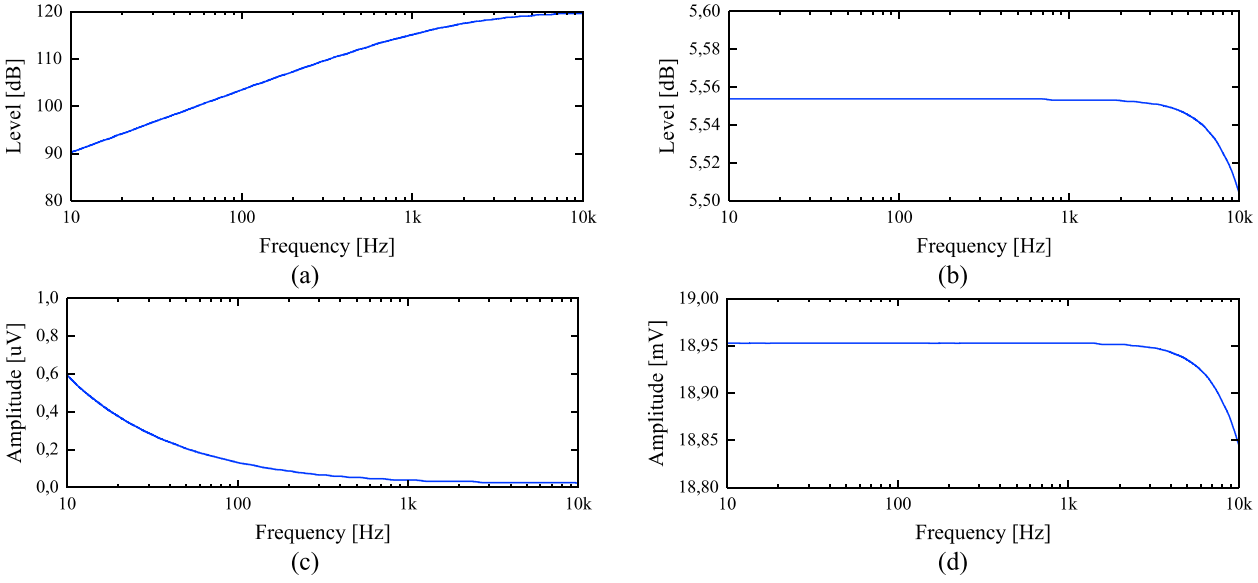

Fig. 5. Simulation results of the op-amp based amplitude demodulator: A – SNR, B – noise figure, C – equivalent input noise voltage spectrum, D – frequency response.

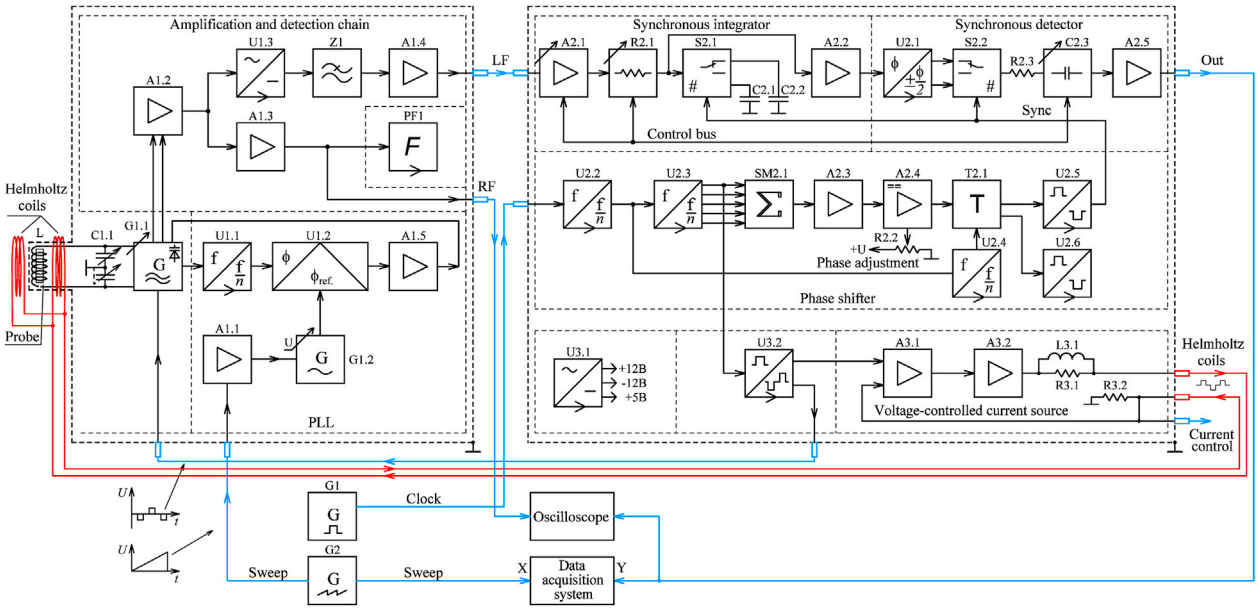

Fig. 6. Block diagram of the proposed NQR sensor: L – probe coil; G1 – clock generator; G2 – sweep generator (sawtooth voltage); A1.1, A1.3 - A1.5 – buffer amplifiers; A1.2 – wideband instrumentation amplifier; C1.1 – ganged capacitor; G1.1 – symmetrical marginal oscillator; G1.2 – voltage-controlled oscillator; PF1 – frequency meter; U1.1 – frequency divider; U1.2 – phase detector; U1.3 – linear active amplitude demodulator; Z1 – low pass filter; U2.1 – phase splitter; U2.2, U2.3 – frequency dividers; U2.4 – binary counter; U2.5, U2.6 - triggers; S2.1, S2.2 – switches; SM2.1 – adder; A2.1-A2.3, A2.5 – amplifiers; A2.4 – comparator, C2.3 – capacitor bank; A3.1 – operational amplifier; A3.2 – power amplifier; U3.1 – power supply module; U3.2 – bipolar pulse generator.

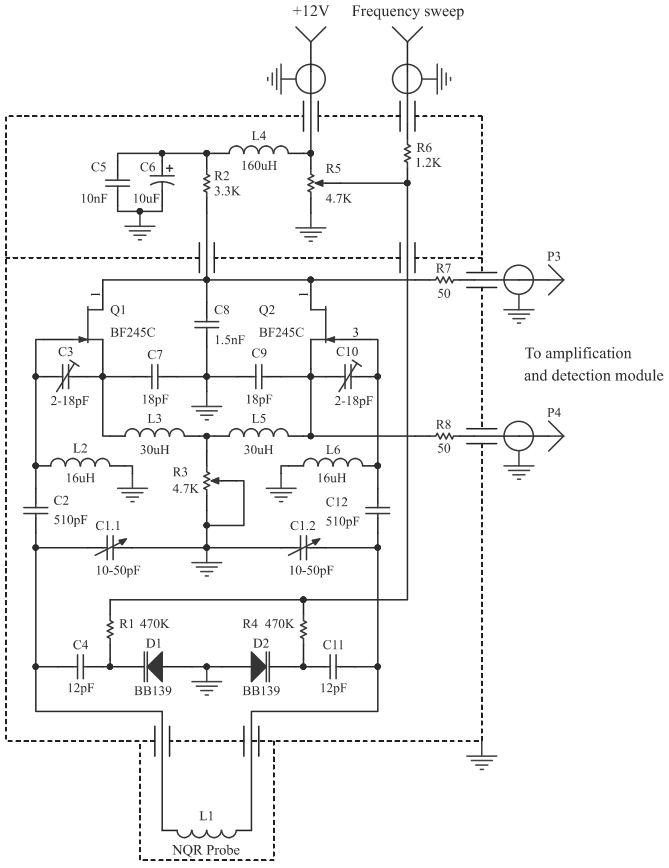

Fig. 7. Circuit diagram of the symmetrical marginal oscillator.

feedback created by a symmetric divider with C3, C7, C9, C10. Input capacitors of JFETs, which are formed by a gate-source transition, are functionally included in the divider. In fact, the circuit of this marginal oscillator is a combination of two oscillators based on a capacitive triple that operate in antiphase. The mode of operation of transistors Q1, Q2 is set by changing the gate-source voltage U_{gs} using potentiometer R3. The frequency of the generated oscillations is determined mainly by the inductance of the coil L1, capacitors C1, C4, C11 and varicaps D1, D2. The circuit generates oscillations in the range of 1–150 MHz. The level of RF voltage on the circuit is in the range of 10 mV–0.5 V. The amplitude of the high-frequence voltage on the oscillatory circuit is set by the ratio of the capacitances of the dividers and is regulated by the synchronous change of capacities C3 and C10. Varicaps D1 and D2 are introduced into the circuit for frequency sweep and implementation of the frequency modulation mode.

The test sample is placed in the inductor coil L1. To be able to work in the low-temperature range, it is necessary to move the coil with the sample into the cooling tank, which is possible when using a communication line. Since the circuit is symmetrical, we used a two-wire symmetrical communication line. The design parameters of the communication line affect its characteristic impedance, and with increasing frequency, they also affect the Q-factor of the circuit. Variable inductors and different types of lines were used to operate in a wide range of frequencies. In particular, experiments were performed using a four-wire symmetrical line, two additional wires of which are connected in parallel to the main ones, but placed in the intersecting planes. This made it possible to reduce the parasitic inductance, which is included in the equivalent circuit of the generator oscillatory circuit. The latter is equivalent to increasing the effective fill factor of the oscillatory circuit coil and increasing the Q-factor. As a result of using a four-wire line, the sensitivity of the detector increased by a factor of 1.8–2.2, and the upper limit of the generated frequencies increased by a factor of 1.2–1.5. Also, to reduce the influence of line characteristics on the resonant characteristics of the circuit when operating at cut-off frequencies (about 150 MHz), we used a constructive line solution, which consists in the use of additional coaxial capacitors placed on the line conductors near the coil with the sample. In this case, the inner linings of the tanks are formed by the conductors of the line, and the outer – by hollow thin-walled cylinders, fixed to the conductors of the line through the dielectric gaskets. Each of the outer linings was connected to the opposite line conductor.

In the study of ^{63}Cu NQR in the vicinity of a relatively low frequency of 26 MHz, an L1 inductor coil was used with the following parameters: inductance – 1.7 uH, coil diameter – 18 mm, coil length – 25 mm, number of turns – 12, winding step – 2.1 mm. A classic symmetrical two-wire communication line with a length of 100 mm and a distance between the conductors of 11 mm is used to connect the L1 coil to the circuit. The inductor coil and line are made of silver-plated copper wire with a diameter of 2 mm. The characteristic impedance of the line used is 276 Ω, which agrees well with the characteristic resistance of the circuit – 278 Ω.

The inner part of the circuit, highlighted by a dotted line, is located in a separate additional screen and suspended on shock absorbers to reduce acoustic and vibration noise.

3.2. Frequency sweep linearization

Scanning of the oscillator frequency near the resonance conditions is carried out using varicaps D1 and D2 (Fig. 7), the nonlinearity of the volt-farad characteristics of which leads to a violation of frequency scale nonlinearity, and, accordingly, to distortion of the resonant spectra.

One solution to this problem is to synchronize the frequency of the marginal oscillator with an external reference oscillator [10]. The disadvantage of this method is the synchronization in a small frequency range and the reduction of marginal oscillator sensitivity. Expansion of the synchronization range while maintaining high sensitivity of marginal oscillator is possible when using phase-locked loop (PLL) [23].

3.3. Amplification and detection chain

RF oscillations from the output of the marginal oscillator are fed to the input of the amplification and detection chain which is schematically shown in Fig. 8.

To ensure minimal influence on the marginal oscillator, the input stage of the circuit, which acts as a RF matching amplifier, is made on broadband op amp AD812 (U1 and U2) with high input resistance and low input capacitance. Op amps are connected according to the instrumentation amplifier circuit, which provides an additional increase in the input resistance of the circuit and the ability to amplify the differential signals. The family of experimental transfer characteristics of the RF path for the frequencies 10 MHz, 30 MHz and 50 MHz is shown in Fig. 9A. A test sinusoidal signal in the frequency range of 10–50 MHz was fed from the OWON AG2052F signal generator to the input of the device under test. At the output of the generator, a 40 dB attenuator is applied to attenuate the amplitude of the test signal. The amplitudes of the signals at the input and output of the device under test were monitored using a Siglent SDS1202CNL digital oscilloscope. The experimental transfer characteristic of the amplitude demodulator on U3 is shown in Fig. 9B. The high linearity of the characteristics of the proposed amplification and detection device allows reducing the distortion of the shape of the resonant lines in the operating frequency range, and the uniformity of the phase-frequency characteristic simplifies the phase adjustment of the synchronous detector. The overall gain of the chain is 53.2 dB.

3.4. Magnetic field modulator with a "rectangular" shape of the output current

A method for observing NQR by magnetic field modulation in the form of rectangular pulses was proposed in Ref. [24]. Nuclear quadrupole resonance lines in powder samples usually expand in the presence of a weak (compared to quadrupole interaction) external magnetic field. This phenomenon is used as a modulation mechanism in NQR spectroscopy and is called the Zeeman modulation. If a bipolar magnetic field is applied to the sample so that the resonance periodically switches between the undisturbed line and the Zeeman expansion, then during the cycle of the magnetic field the NQR signal is jammed twice. The resulting amplitude modulation of the RF signal is detected by a lock-in amplifier at double the Zeeman modulation frequency [25]. An important feature of the Zeeman modulation, in comparison with frequency modulation, which is also used in the NQR technique, is the insensitivity of the spectrometer to piezoelectric resonances and the absence of parasitic amplitude modulation of the RF signal. At the same time, direct interference to the coil of the sensor circuit at the second harmonic of the modulation frequency is eliminated.

Magnetic field is created by two coils having a common axial axis and located in parallel planes at a distance equal to their radius (Helmholtz coils).

Voltage-controlled current sources (VCCS) are designed to supply a load with a current whose strength does not depend on the output voltage, but is regulated only by the magnitude of the input voltage of the circuit. The feature of a voltage-controlled current source is its high output resistance. A simplified diagram of the proposed magnetic field modulator based on VCCS is shown in Fig. 10 [26]. The basis of the circuit is an operational amplifier U1 with connected high-power MOSFETs Q1 – Q8. The use of MOSFETs in the circuit is due to the low resistance of the chain in contrast to bipolar ones and, accordingly, lower heat release.

The depth of the current feedback is regulated by the selection of resistors R3 and R14. In this case, both the control signal (bipolar voltage) and the feedback signal from the resistor R16 are fed to the inverting input U1. To prevent high-frequency excitation, the L1 and R15 are connected in series with the load. The proposed activation of

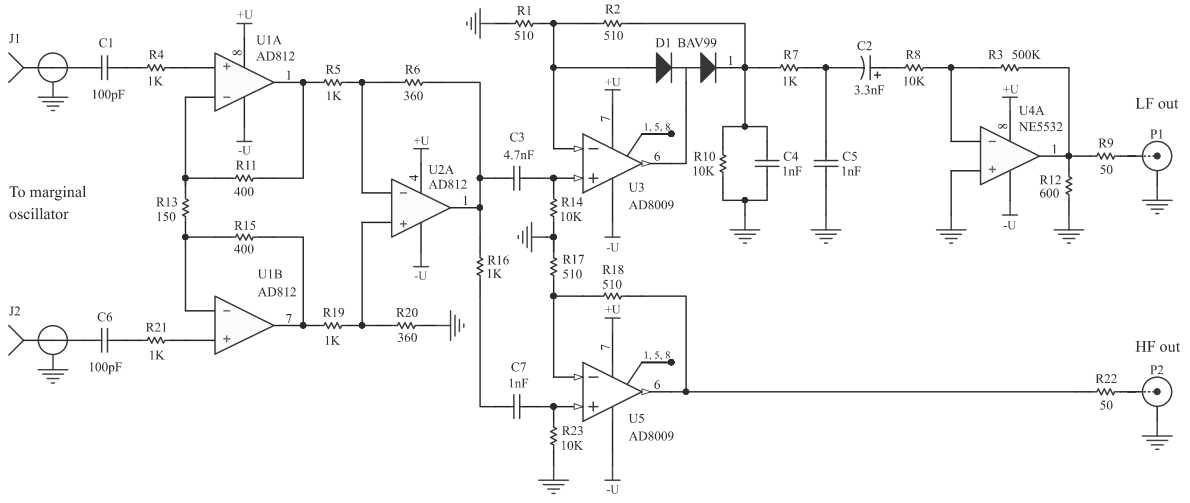

Fig. 8. Circuit diagram of the amplification and detection chain.

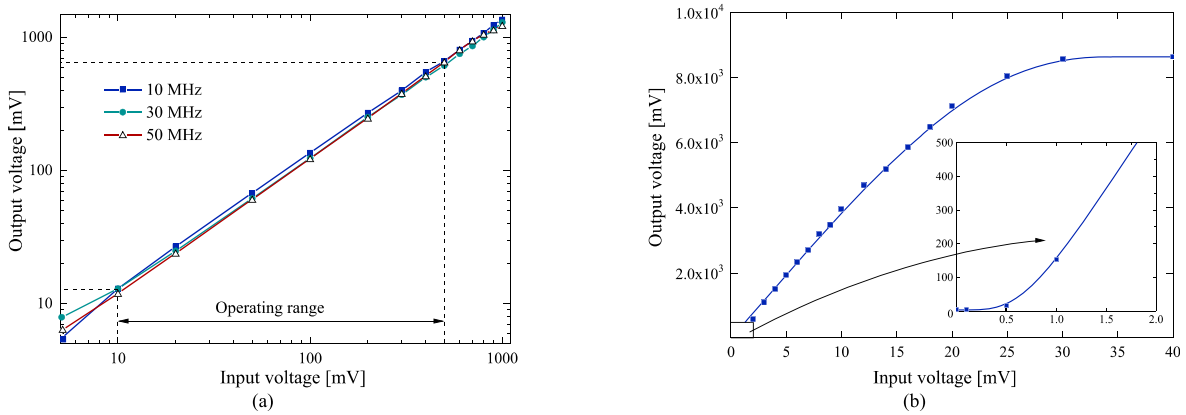

Fig. 9. Experimental studies of the amplification and detection chain: A – RF chain transfer characteristics, B – transfer characteristic of the amplitude demodulator.

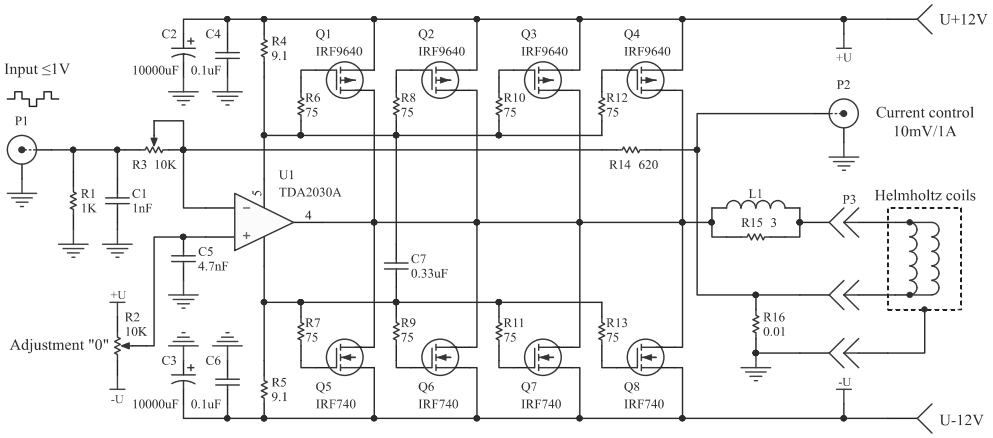

Fig. 10. Circuit diagram of the VCCS based magnetic field modulator.

transistors VT1 – VT8 allows unloading the output of the operational amplifier and using transistors in sparing mode.

The Helmholtz coils Lm are used as modulator load. With a series connection, the maximum induction of the magnetic field in the coils reaches ±100 G at a current of ~30 A. To achieve the required value of magnetic field induction, the design parameters of Helmholtz coils were calculated: average radius – 5 cm, active resistance of each coil – 0.1 Ω, inductance of one coil – 110 uH. Experimental studies showed that the inhomogeneity of the magnetic field in the area of the sample did not exceed 0.1%. Fig. 11 shows current waveforms in the Helmholtz coils with the feedback off and on. The experimental waveforms obtained using the Siglent SDS1202CNL oscilloscope. When the feedback was turned off, the coil current rise/fall time was 1.2 ms, and when it was turned on, it was 0.2 ms. To visualize the shape of the current in the load and control its level, the resistance R16 is calibrated and is 0.01 ± 5% Ω.

3.5. Signal processing chain

A system with phase detection of the response signal was used to study the NQR spectra in sweep mode. This allows you to ensure good reproducibility of the line shape. The method of synchronous detection, together with such methods as stroboscopic and multichannel accumulation, is widely used to extract weak signals from noise in experimental physics. It is especially actively used in optical and radio spectroscopy [27].

To implement the method of synchronous detection, in this work we have developed a circuit diagram of the absorption signals processing chain consisting of: synchronous detector, synchronous integrator and phase shifter.

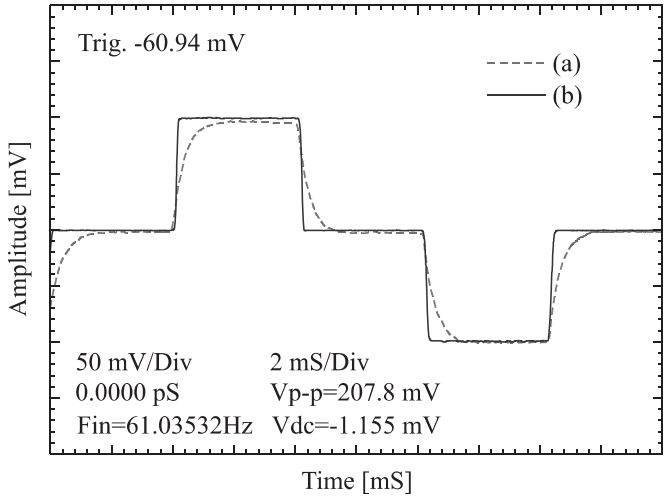

Fig. 11. Influence of feedback on the shape of current in inductive load: A – feedback is disabled, B – feedback is enabled (VCCS mode).

A circuit diagram of a synchronous integrator developed for an NQR sensor is shown in Fig. 12. The on-off switch U4, alternately, with a frequency *f* connects the capacitors to one of the resistors R with the help of a switching bipolar pulse U_g.

In this case, the output voltage U_{out} will be the result of the successive integration of U_{in} by the links RC7 and RC8. If the input voltage U_{in} is a rectangular signal with a frequency *F,* which coincides with the switching

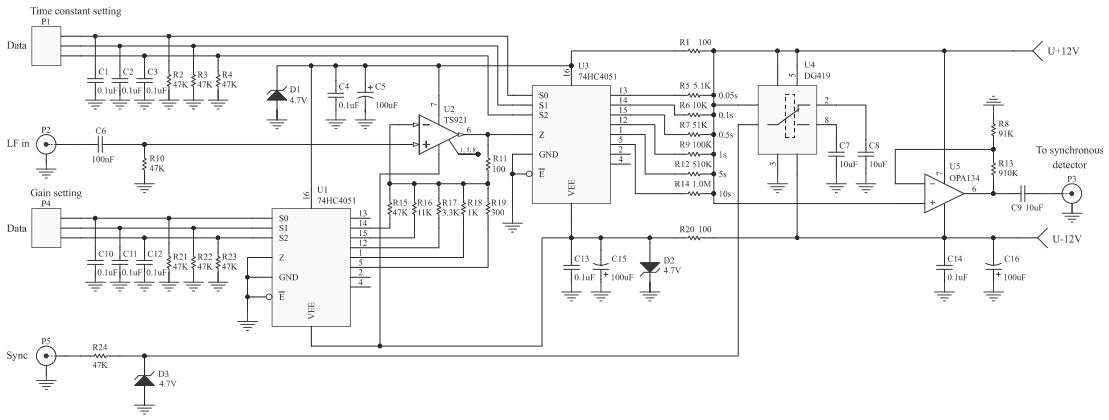

Fig. 12. Circuit diagram of the synchronous integrator.

frequency of the switch *f* and the amplitude U_{in}, then it is clear that C7 will be charged to the voltage + U_{out}, and C8 to the voltage -U_{out}. Since | U_{out}| is the voltage across each capacitor, then a rectangular signal with amplitude U_{out} is obtained at the output.

The frequency response of a synchronous filter, in addition to the passband near the zero frequency, also has a number of bands at frequencies that are multiples of the switching frequency. At frequencies 2*F*, the transmission coefficient is zero, that is, the odd harmonics of the signal are passed, and the paired ones are suppressed. The input signal is amplified by TS921 op amp, the gain of which is set by resistors R15 – R19. The resistors are connected to the op amp feedback circuit by the multiplexer U1. The multiplexer U3 switches the resistors R5 – R7, R9, R12, R14, which set the integration time constant in the range of 0.05–10 s. The analog switch U4 according to the synchronization signal connects the capacitors C7 and C8 to the resistor matrix.

Fig. 13 is a dependence showing a sharp increase in SNR at the output of a synchronous detector while narrowing the integrator bandwidth (82 dB for a 1 Hz band). Dependences shown in Fig. 13B characterize the transfer characteristics of a synchronous detector with an integrator time constant of 0.51×10^{-3} s. The non-linearity of the transfer characteristic of a synchronous detector is ~1% for frequencies 50 Hz, 100 Hz, 200 Hz.

3.6. Observation of ^{69}Cu NQR in thermometric substance Cu_2O

When developing secondary temperature standards based on the NQR method, it is important to minimize the temperature gradient in the sample, which leads to a narrowing of the spectral line and makes it possible to significantly increase the accuracy of temperature measurement [28,29]. Potassium trioxochlorate is used as the thermometric substance of most NQR temperature sensors [30–33]. Such sensors have a number of disadvantages, in particular, the nonlinear dependence of the NQR frequency on the measured temperature. When performing experiments with the substance $KClO_3$, it should be borne in mind that its mixtures with organic substances are explosive, sensitive to friction, impact, heat. It is especially easy to explode chlorates in a mixture with sulfur, red phosphorus, antimony, starch, soot, sugar. When mixing Berthollet salt with ammonium salts, a product is formed, which explodes at 100 °C, and during prolonged storage is self-igniting. This was one of the good reasons not to conduct research with this substance. Copper oxide was used as the thermometric substance of the proposed NQR sensor, which is characterized by a strong temperature dependence of the resonance frequency of ^{63}Cu NQR (up to ~3.18 kHz/K in the temperature range 77–300 K) [33,34]. For research, we used polycrystalline plates of pressed Cu_2O powder with a thickness of 0.4 mm and an area of 6 × 6 mm^2.

The calculation of the operating frequency of the marginal oscillator was performed according to the formula that correlates the frequency (ν_0) of NQR and the temperature *(T)* of the thermometric substance Cu_2O [35,36]:

$$\nu_0(T,P) = \nu_Q^0(P)\left\{1+\lambda(P)\Theta(P)\left(\frac{\exp\left(\frac{\Theta(P)}{T}\right)}{1-\exp\left(\frac{\Theta(P)}{T}\right)}+\frac{1}{2}\right)\right\} = \nu_Q^0(P)\left\{1-\frac{\lambda(P)\Theta(P)}{2}\coth\left(\frac{\Theta(P)}{2T}\right)\right\} \quad (8)$$

At atmospheric pressure P_{atm} = 101.325 kPa we consider the following constants: $^{63}\nu_Q^{(0)}$ (P_{atm}) = 27.0513 MHz is the *T*-independent coefficient, $\Theta(P_{atm})$ = 0.00012978 K^{-1} is the characteristic temperature for the relevant phonon mode, $\lambda(P_{atm})$ = 135.3 K is the coupling constant between the phonon and electric field gradient [35].

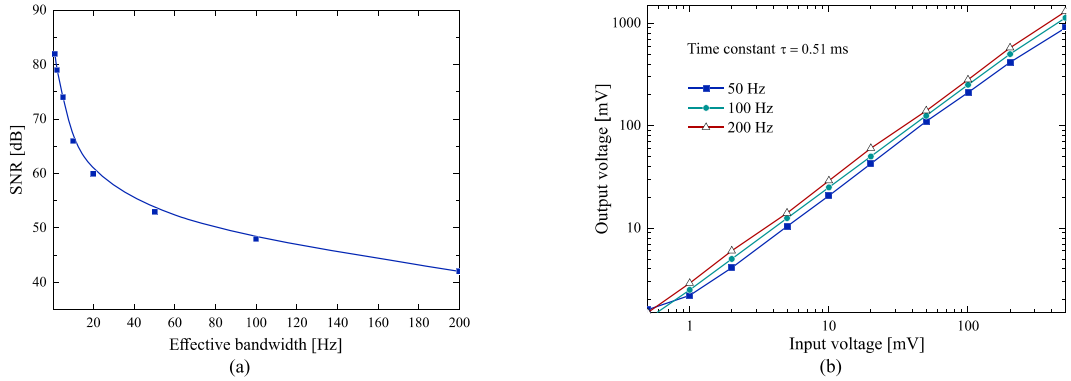

Fig. 13. Experimental studies of the signal processing chain: A – dependence of the SNR at the output of the synchronous detector on the integrator bandwidth.; B – transfer characteristics of the synchronous detector for frequencies: 50 Hz, 100 Hz, 200 Hz.

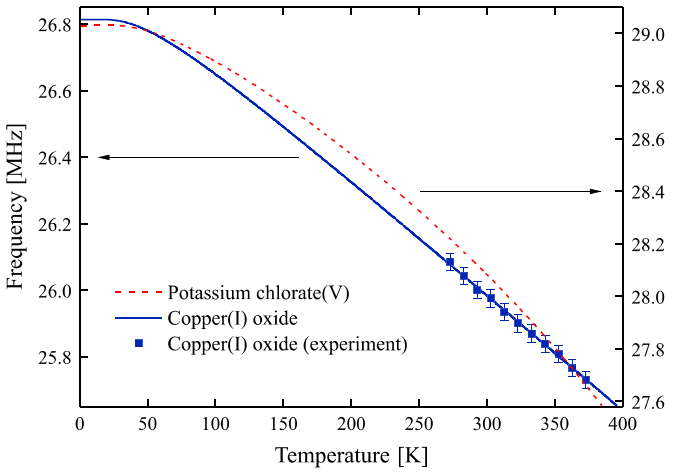

Fig. 14. Temperature dependences of the NQR frequencies for ^{35}Cl and ^{63}Cu isotopes.

The dependence of the ^{63}Cu NQR frequency in Cu_2O on the temperature $\nu_0(T)$ for the temperature range of 4–400 K, calculated by formula (8), is shown in Fig. 14 (solid line). As we can see, the limiting frequency values are 25.65 MHz and 26.82 MHz. For comparison, the calculated temperature dependence of the ^{35}Cl NQR frequency in $KClO_3$ is also shown (Fig. 14, dashed line). Unlike ^{35}Cl NQR in $KClO_3$, for cuprous oxide, the temperature dependence of the ^{63}Cu NQR frequency in the frequency range 26.621–25.658 MHz is linear in the temperature range of 100–390 K.

To achieve maximum SNR, it is necessary that the coil fill factor with the sample was maximum. However, in this case, the temperature gradient of the sample may increase, which will lead to the expansion of the spectral line. That is why we conducted a study of the minimum mass of the sample whereby it is possible to observe the NQR signal with a satisfactory SNR. Previous studies have also shown that the spectral line width and temperature coefficient are almost independent of the age of the sample. To determine the transfer characteristic of the proposed NQR sensor, a number of measurements of ^{63}Cu NQR spectra were performed for cuprous oxide samples of different masses. Fig. 15 shows the results obtained for samples weighing from 0.2 g to 2 g, recorded at 26.006 MHz at a temperature of 293 K. The experiments were performed at an integrator band of 100 Hz. In this case, the maximum SNR of the channel was about 48 dB, and the maximum SNR of the spectrum was 23.5 dB (at a sample weight of 2 g). The recording time of one spectrum was about 5 min. The minimum mass of the thermometric substance Cu_2O, recorded without the use of digital accumulation and averaging algorithms, was

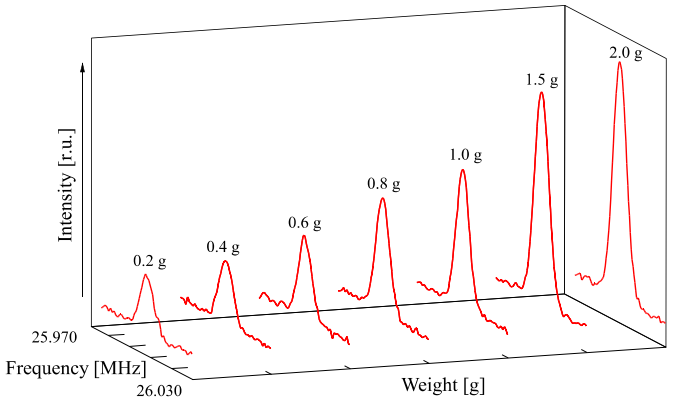

Fig. 15. NQR spectra for ^{63}Cu isotope in Cu_2O samples of various weights.

200 mg with an SNR of 9.1 dB. For a sample weighing 200 mg, the width of the spectral line at half its maximum intensity was 5 kHz, and the measurement accuracy in the room temperature range was 0.03 K. The NQR signal is recorded at the second harmonic of the modulation frequency using a symmetric marginal oscillator and a linear amplitude demodulator. The modulation frequency of the magnetic field was 65 Hz, and its induction was 7 G.

With certain modifications of the input circuit of the proposed sensor and a change of its operating modes, one can also use other compounds that are characterized by the temperature dependence of the NQR frequency, such as Sb_2S_3, GaSe, InSe and others.

4. Conclusions

There are stationary and pulsed methods for observing NQR signals in the frequency range from ~2 to 1000 MHz. The paper describes development of the detailed structure and circuit diagrams of the continuous wave NQR temperature sensor with increased conversion linearity.

The SPICE models of known circuit diagrams of amplitude demodulators of NQR marginal oscillators have been studied. A circuit diagram of a symmetric marginal oscillator with a linear active demodulator has been developed. It is established that at amplitude modulation of 40% and change of input voltage in the range of 20–1000 mV the above circuit diagram provides better linearity of transfer characteristic (harmonic factor of the output voltage did not exceed 0.5%) than the transistor and diode demodulators.

To implement the Zeeman modulation in NQR, the circuit diagram for an amplifier based on a controlled current source is developed providing magnetic field induction in the working area of the Helmholtz coils up to ±100 G.

A signals processing chain for continuous wave NQR temperature sensor with separate setting of the bandpass is proposed: 0.01–20 Hz for a synchronous integrator and 0.1–50 Hz for a synchronous detector, which provides the best adjustment of the conditions for detecting a resonant signal when observing isotopes with different values of nuclear spin relaxation.

The purpose of the experiment was to determine the minimum mass of a thermometric substance which can be precisely detected using the proposed NQR sensor. Cuprous oxide (Cu_2O) was chosen as the research object of the proposed temperature sensor. To a large extent, this choice is due to the ability to provide a high frequency of cuprous oxide, which in turn provides high reproducibility of the width of the response signal line, as well as a relatively narrow width of the absorption line (~10 kHz) and high temperature sensitivity ~4–5 kHz/°C. From the results of the research obtained with the help of the developed NQR sensor, it was established that cuprous oxide is a promising material for use in secondary temperature standards. It is confirmed that the temperature dependence of the ^{63}Cu NQR frequency in the frequency range 26.621–25.658 MHz is linear in the temperature range 100–390 K. The experiments were performed at an integrator band of 100 Hz. In this case, the maximum SNR of the channel was about 48 dB, and the maximum SNR of the spectrum was 23.5 dB (at a sample weight of 2 g). The recording time of one spectrum was about 5 min. It has been experimentally confirmed that the use of a low-mass sample (less than 200 mg) as a thermometric substance of the proposed NQR sensor is quite sufficient for successfully observation of the resonance line at the SNR equal to 9.1 dB. For a sample weighing 200 mg, the width of the spectral line at half its maximum intensity was 5 kHz, and the measurement accuracy in the room temperature range was 0.03 K.

Declaration of competing interest

The authors declare that they have no known competing financial interests or personal relationships that could have appeared to influence the work reported in this paper.

Acknowledgements

This work was supported by the Ministry of Education and Science of Ukraine (grant No 18.801, state registration number 0120U101249).

References

[1] J. Vanier, Temperature dependence of the pure nuclear quadrupole resonance frequency in KClO3, Can. J. Phys. 38 (1960) 1397.
[2] F.N.H. Robinson, Frequency modulated NMR oscillator without amplitude modulation, Rev. Sci. Instrum. 34 (1963) 1260.
[3] A. Other, H. Iwaoka, A precision on nuclear quadrupole resonance thermometer, IEEE Trans. Ins. Meas. 4 (1976) 357–362.
[4] V.P. Anferov, O.N. Bryuchanov, V.S. Grechishkin, T.N. Rudakov, A nuclear quadrupole resonance thermometer with frequency locking, J. Mol. Struct. 83 (1982) 365–368.
[5] John C. Lindon, Encyclopedia of Spectroscopy and Spectrometry, Academic Press, Oxford, 2010.
[6] B.H. Suits, Nuclear Quadrupole Resonance Spectroscopy: Handbook of Applied Solid State Spectroscopy, Springer, Boston, 2006.
[7] P.A. Probst, B. Collet, W.M. MacInnes, Marginal oscillator optimized for radiofrequency size effect measurements, Rev. Sci. Instrum. 47 (1976) 1522–1526, https://doi.org/10.1063/1.1134568.
[8] Shinho Cho, Sung Ho, Choh, A nuclear quadrupole resonance spectrometer from 2 to ~50 MHz, J. Kor. Phys. Soc. 21 (1988) 399–404.
[9] O.S. Stoican, NQR detection setup, Rom. J. Phys. 51 (2006) 311–315.
[10] B. Makarov, V. Ryzhov, Advance of Marginal Oscillator, RuPAC-2010, Protvino, Russia, 2010, pp. 122–124.
[11] M. Ivanchuk, V. Brajlovskyj, Automated nuclear quadruple resonance spectrometer, Adv. Electr. Comput. Eng. 8 (2008) 29–31, https://doi.org/10.4316/aece.2008.02005.
[12] O.Z. Hotra, A.P. Samila, G.M. Rozorinov, O.V. Gres, Current status and development prospects of nuclear quadrupole resonance pulsed spectroscopy methods: a review, Telecommun. Radio Eng. 78 (2019) 1483–1496, https://doi.org/10.1615/TelecomRadEng.v78.i16.60.
[13] A.P. Samila, G.I. Lastivka, Yu V. Tanasyuk, Actual problems of computer parametric identification of the NMR and NQR spectra: a review, J. Nano- Electron. Phys. 11 (2019) 1–10, https://doi.org/10.21272/jnep.11(5).05036, 05036.
[14] A. Doll, Pulsed and continuous-wave magnetic resonance spectroscopy using a low-cost software-defined radio, AIP Adv. 9 (2019) 115110–115111, https://doi.org/10.1063/1.5127746. –13.
[15] Michael I. Newton, Edward A. Breeds, Robert H. Morris, Advances in electronics prompt a fresh look at continuous wave (CW) nuclear magnetic resonance (NMR), Electronics 6 (2017) 89–91, https://doi.org/10.3390/electronics6040089. –21.
[16] A. Gauzzi, J. Le Cochec, G. Lamura, B.J. Jonsson, V.A. Gasparov, F.R. Ladan, B. Placais, P.A. Probst, D. Pavuna, J. Bok, Very high resolution measurement of the penetration depth of superconductors by a novel single-coil inductance technique, Rev. Sci. Instrum. 71 (2000) 2147–2153, https://doi.org/10.1063/1.1150597.
[17] Stephen A. Hall, Michael A. Pusateri, Jeffrey L. Schiano, Labview based frequency counter and voltmeter for a continuous-wave quadrupole resonance spectrometer, Annu. Res. J. 3 (2005) 187–196.
[18] V.V. Brayilovs'kyy, A.P. Samila, O.G. Khandozhko, Spin-detektor YaKR termometra [Spin detector for NQR thermometer], Meassuring and computing devices in technological processes 1 (2009) 43–46 (in Ukrainian).
[19] V.V. Brailovs'kiy, A.P. Samila, O.G. Khandozhko, Datchik signalov yadernogo kvadrupol'nogo rezonansa [Nuclear quadrupole resonance sensor], Pribory i tehnika èksperimenta 2 (2010) 177 (in Russian).
[20] V.V. Brayilovs'kyy, A.P. Samila, O.G. Khandozhko, Avtodynnyy davach syhnaliv YaKR ta YaMR [Autodyne sensor for NQR and NMR signals], Sens. Electron. Microsyst. Technol. 1 (2010) 20–24 (in Ukrainian).
[21] L.F. Politansky, A.P. Samila, V.A. Khandozhko, Analiz shumovyh kharakteristik avtodinnogo spin-detektora [Analysis of the noise characteristics of an autodyne spin detector], Visnik NTU «HPI». 68 (2012) 104–110 (in Russian).
[22] G.B. Furman, S.D. Goren, Pure NQR quantum computing, Z. Naturforsch. 57a (2002) 315–319, https://doi.org/10.1515/zna-2002-6-705.
[23] A.P. Samila, A.G. Khandozhko, V.A. Khandozhko, Avtodinnyy spektrometr yadernogo kvadrupol'nogo rezonansa s ravnomernoy chastotnoy shkaloy [The continuous wave NQR spectrometer with equidistant frequency scale], Tekhnologiya i Konstruirovanie v Elektronnoi Apparature 5–6 (2010) 17–22 (in Russian).
[24] G.D. Watkins, R.V. Pound, The pure nuclear electric quadrupole resonance of N14 in three molecular, solids, Phys. Rev. 85 (1952) 1062.
[25] D. Mao, G.L. Petersen, P.J. Bray, A bi-symmetric square wave Zeeman modulator for nuclear quadrupole resonance, Solid State Nucl. Magn. Reson. 1 (1992) 227–230.
[26] A.P. Samila, A.G. Khandozhko, V.A. Khandozhko, Zeyeman-modulyator s pretsizionnoy formoy vykhodnogo toka [Zeeman modulator with precision output current waveform], E. Eur. J. Enterprise Technol. 1 (2011) 40–43 (in Russian).
[27] M. Dhanalakshmi, K. Rukmani, A lock-in amplifier suitable for NMR and NQR spectrometers, J. Instrum. Soc. India. 36, 153-158.
[28] K.B. Dillon, Nuclear quadrupole resonance spectroscopy, in: Spectroscopic Properties of Inorganic and Organometallic Compounds, vol. 38, 2006, pp. 173–188.
[29] V.D. Karpenko, N.O. Koval'chuk, A.M. Lenovenko, S.D. Solod, A.G. Suvorov, Sovremennoye sostoyaniye i perspektivy yaderno-kvadrupol'noy rezonansnoy termometrii Ukrainy [Current state and prospects of nuclear-quadrupole resonance thermometry in Ukraine], Space Technology, Missile Armaments 2 (2017) 146–150 (in Russian).
[30] A. Lenovenko, B. Stadnyk, P. Stolyarchuk, V. Parakuda, N. Koval'chuk, Vymiryuval'nyy kompleks dlya kalibruvannya, perevirky i atestatsiyi zasobiv vymiryuvannya temperatury na bazi etalonnoho yaderno-kvadrupol'noho termometra pershoho rozryadu ЯКРТ-5М [Measuring complex for calibration, inspection and certification of temperature measuring instruments based on the reference nuclear-quadrupole thermometer of the first category ЯКРТ-5М], Measur. Equip. Metrol. 74 (2013) 127–131 (in Ukrainian).
[31] S.N. Popov, 35Cl nuclear quadrupole resonance and the macroscopic superstructure in Hg2Cl2 crystal, Phys. Solid State 39 (1997) 1143–1146, https://doi.org/10.1134/1.1130032.
[32] R. Volyts'kyy, Metod pobudovy yaderno-kvadrupol'noho rezonansnoho termometra na osnovi tsyfrovykh syntezatoriv [A method for constructing a nuclear-quadrupole resonance thermometer based on digital synthesizers], Measur. Equip. Metrol. 74 (2013) 12–15 (in Ukrainian).
[33] R. Sh Lotfullin, A.A. Boguslavsky, R.V. Magera, Temperaturnaya zavisimost chastoty kvadrupolnogo rezonansa 35Cl v KClO3 i 63Cu v Cu2O [Temperature dependence of the quadrupole resonance frequency 35Cl in KClO3 and 63Cu in Cu2O], Izvestiya AN SSSR: seriya fizika 39 (1975) 2497–2504 (in Russian).
[34] Weller Matthias, NMR/NQR studies at very low temperatures and high pressures in strongly correlated electron systems, Diss. ETH 17290 (2008).
[35] Kentaro Kitagawa, Hirotada Gotou, Takehiko Yagi, Atsushi Yamada, Takehiko Matsumoto, Yoshiya Uwatoko, Masashi Takigawa, Space efficient opposed-anvil high-pressure cell and its application to optical and NMR measurements up to 9 GPa, J. Phys. Soc. Jpn. 79 (2010) 1–8, https://doi.org/10.1143/JPSJ.79.024001, 024001.
[36] A.P. Reyes, E.T. Ahrens, R.H. Heffner, P.C. Hammel, J.D. Thompson, Cuprous oxide manometer for high-pressure magnetic resonance experiments, Rev. Sci. Instrum. 63 (1992) 3120–3122, https://doi.org/10.1063/1.1142564.